

# Fabricating low cost and high performance elastomer lenses using hanging droplets

W. M. Lee,<sup>1,2,3,\*</sup> A. Upadhy,<sup>1</sup> P. J. Reece,<sup>2</sup> and Tri Giang Phan<sup>3,4</sup>

<sup>1</sup> Research School of Engineering, College of Engineering and Computer Science, Australia National University, North Road, Canberra ACT 0200 Australia

<sup>2</sup> School of Physics, UNSW Australia, Sydney, NSW 2035, Australia

<sup>3</sup> Garvan Institute of Medical Research, 384 Victoria Street, Darlinghurst, NSW 2010 Australia

<sup>4</sup> Faculty of Medicine, UNSW Australia, 384 Victoria Street, Darlinghurst, NSW 2010 Australia  
\*steve.lee@anu.edu.au

**Abstract:** Existing methods for low cost lenses using parallel mold stamping and high temperature reflow requires complex engineering controls to produce high quality lenses. These manufacturing techniques rely on expensive equipment. In this paper, we propose a low cost (< \$ 0.01 per pc) flexible moldless lens fabrication method based on curing a hanging transparent polydimethylsiloxane (PDMS) elastomer droplet on a curved substrate. Additional deposition of hanging droplets in the same manner led to a substantial increase in the lens curvature and concomitant decrease in the focal length of the PDMS lenses down to ~2 mm. The shortest focal length lenses were shown to collimate light from a bare light emitting diode (LED) and image microscopic structures down to around 4  $\mu\text{m}$  with 160x magnification. Our hanging droplet lens fabrication technique heralds a new paradigm in the manufacture of low cost, high performance optical lenses for the masses. Using these lenses, we were able to transform an ordinary commercial smartphone camera into a low-cost digital dermascope (60x magnification) that can readily visualize microscopic structures on skin such as sweat pores.

©2014 Optical Society of America

**OCIS codes:** (220.4610) Optical fabrication; (120.0120) Instrumentation, measurement, and metrology; (110.0110) Imaging systems; (180.0180) Microscopy

## References and links

1. P. Tolley, "Polymer optics gain respect," *Photon. Spectra* **37**, 76–79 (2003).
2. S. W. Menzies, J. Emery, M. Staples, S. Davies, B. McAvoy, J. Fletcher, K. R. Shahid, G. Reid, M. Avramidis, A. M. Ward, R. C. Burton, and J. M. Elwood, "Impact of dermoscopy and short-term sequential digital dermoscopy imaging for the management of pigmented lesions in primary care: a sequential intervention trial," *Br. J. Dermatol.* **161**(6), 1270–1277 (2009).
3. L. Bellina and E. Missoni, "Mobile cell-phones (M-phones) in telemicroscopy: increasing connectivity of isolated laboratories," *Diagn. Pathol.* **4**(1), 19 (2009).
4. O. Mudanyali, D. Tseng, C. Oh, S. O. Isikman, I. Sencan, W. Bishara, C. Oztoprak, S. K. Seo, B. Khademhosseini, and A. Ozcan, "Compact, light-weight and cost-effective microscope based on lensless incoherent holography for telemedicine applications," *Lab Chip* **10**(11), 1417–1428 (2010).
5. E. Linder, A. Grote, S. Varjo, N. Linder, M. Lebbad, M. Lundin, V. Diwan, J. Hannuksela, and J. Lundin, "On-Chip Imaging of *Schistosoma haematobium* Eggs in Urine for Diagnosis by Computer Vision," *PLoS Negl. Trop. Dis.* **7**(12), e2547 (2013).
6. D. N. Breslau, R. N. Maamari, N. A. Switz, W. A. Lam, and D. A. Fletcher, "Mobile Phone Based Clinical Microscopy for Global Health Applications," *PLoS ONE* **4**(7), e6320 (2009).
7. H. Zhu, S. O. Isikman, O. Mudanyali, A. Greenbaum, and A. Ozcan, "Optical imaging techniques for point-of-care diagnostics," *Lab Chip* **13**(1), 51–67 (2012).
8. X.-H. Lee, I. Moreno, and C.-C. Sun, "High-performance LED street lighting using microlens arrays," *Opt. Express* **21**(9), 10612–10621 (2013).
9. P. J. Gramann and T. A. Osswald, *Injection Molding Handbook* (Hanser Gardner Publication Inc, Cincinnati, 2002).
10. J. L. Wilbur, R. J. Jackman, G. M. Whitesides, E. L. Cheung, L. K. Lee, and M. G. Prentiss, "Elastomeric optics," *Chem. Mater.* **8**(7), 1380–1385 (1996).
11. Y. Gambin, O. Legrand, and S. R. Quake, "Microfabricated rubber microscope using soft solid immersion lenses," *Appl. Phys. Lett.* **88**(17), 174102 (2006).

12. K. H. Jeong, J. Kim, and L. P. Lee, "Biologically inspired artificial compound eyes," *Science* **312**(5773), 557–561 (2006).
13. J. J. Kim, Y. Lee, H. G. Kim, K. J. Choi, H. S. Kweon, S. Park, and K. H. Jeong, "Biologically inspired LED lens from cuticular nanostructures of firefly lantern," *Proc. Natl. Acad. Sci. U.S.A.* **109**(46), 18674–18678 (2012).
14. Dow Corning Newest Moldable Optical Silicone Further Expands Options for More Energy Efficient and Reliable LED Lighting Designs," (2013), [http://www.dowcorning.com/content/news/Moldable\\_Optical\\_Silicone.aspx](http://www.dowcorning.com/content/news/Moldable_Optical_Silicone.aspx).
15. H. Ren, S. Xu, and S.-T. Wu, "Effects of gravity on the shape of liquid droplets," *Opt. Commun.* **283**(17), 3255–3258 (2010).
16. R. Tadmor, P. Bahadur, A. Leh, H. E. N'guessan, R. Jaini, and L. Dang, "Measurement of Lateral Adhesion Forces at the Interface between a Liquid Drop and a Substrate," *Phys. Rev. Lett.* **103**(26), 266101 (2009).
17. F. A. Chowdhury and K. J. Chau, "Variable focus microscopy using a suspended water droplet," *J. Opt.* **14**(5), 055501 (2012).
18. T. Krupenkin, S. Yang, and P. Mach, "Tunable liquid microlens," *Appl. Phys. Lett.* **82**(3), 316–318 (2003).
19. Z. Bian, S. Dong, and G. Zheng, "Adaptive system correction for robust Fourier ptychographic imaging," *Opt. Express* **21**(26), 32400–32410 (2013).

---

## 1. Introduction

The current demands for light-emitting diodes (LEDs) and miniature complementary metal-oxide semiconductor (CMOS) imaging sensors in consumer and technical fields has spurred the growth in manufacturing low cost optics [1]. In imaging, low cost miniature microscopes have enabled a new generation of mobile microscope devices that is increasingly used in primary telemedicine [2–5] and global healthcare [6, 7]. Furthermore, micro-lens collimators have been shown to have the potential to greatly reduce light pollution and lower electricity consumption [8].

Polymer lenses possess several significant commercial and practical benefits such as low material costs, high optical properties (refractive index  $n \sim 1.57$ – $1.59$ ), flexible shaping (high temperature reflow), and high mechanical resilience. These factors enable polymer lenses to be mass produced at reasonably low cost and high quality. Nevertheless, mold stamping requires investment in costly equipment which relies on multiple complex control parameters governing the production [9]. These factors includes quality of the mold, reflow velocity, injection temperatures and pressures. In addition, polymer fabrication methods can be inefficient [9]. There is therefore a commercial and environmental need to provide alternative lens fabrication technologies that can circumvent the limitations of current lens manufacturing processes and also make it more accessible to the masses.

The advent of elastomeric optics using polydimethylsiloxane (PDMS) [10] has provided a new ingredient and opportunity to construct high performance optical components. PDMS optical elements are generally resilient to high temperatures ( $> 125$  °C), show minimal aging (yellowing), exhibit high transparency ( $> 95\%$ ) within the visible wavelength, high refractive indices ( $n = 1.47$ – $1.55$ ), and low molding temperature ( $< 100$  °C). This means that the lenses can be rapidly fabricated with conventional mold stamping methods and not restricted to high temperature equipment or reflow techniques [10]. Recently, there have been an increasing number of novel applications of elastomeric optics such as rubber microscope [11], bio-inspired wide field lenses [12] and LED anti-reflection shielding [13]. The trend of elastomeric optics are also gaining significant industrial interest [14]. However, they still rely on inefficient mold-based technology and often require precision milling to overcome defects in the stamping.

A hanging droplet is produced when equilibrium is attained between the interfacial energies (liquid, air and solid surface) and gravity [15, 16]. A droplet of water or oil can be used to magnify small structures [15, 17]. Tunable liquid lenses attempts to harness this natural curvature under electrical or mechanical forces for fast focusing [18] which replace the need for a multiple lenses system. The former remains a transient solution and the latter requires complex actuation processes. Nevertheless, it is evident that lensing droplets is flexible and cost efficiency method.

In this paper, we demonstrate a method to produce low cost, high performance lenses by repeatedly adding and curing a hanging PDMS droplet at fixed intervals on a curved PDMS

substrate. The uniform gravitational force exerted over the entire inverted PDMS layer assists in the formation of a well-defined refractive lens that changes its parabolicity. The paper will be structured in the following sections. In sections 2 to 3, we describe increased magnifying power of a hanging droplet and the steps taken to harvest lenses. In this section 2, we shall first illustrate the magnifying power of a single cured hanging droplet versus a horizontally cured droplet in section 2. We will then describe the steps taken to increase the droplet curvature and thereby reducing the focal length of the final PDMS lens during fabrication in section 2.1. In section 3, we test the performance of the PDMS lens for imaging and lighting. For imaging, we measure the smallest resolvable structure in a transmitted light imaging setup. The fabricated PDMS lenses are attached to miniature camera system, containing the imaging lenses. A 1951 USAF resolution card is used as the imaging target. We also compared the imaging quality of the lens against a commercial microscope lens. In Section 4, we constructed a fiber optics light collection platform to measure the emitted light field at different spatial location emerging from an LED light source, with and without the PDMS lenses. Taking advantage of the low cost and high imaging performance of the PDMS lenses, we designed and constructed a complementary mobile microscope device equipped with LEDs and attached that to a smartphone camera. In section 5, we show that our lightweight device ( $\sim 0.5$  g) transformed an ordinary smartphone camera into a powerful dermascope that can resolve single sweat pores at  $\sim 60\times$  magnification.

## **2. Magnifying lenses with a hanging droplet**

In refracting lenses, light bends along a transparent curved surface due to the differences in refractive index along the interface. The radius of curvature of a thin lens can have different degree of parabolicity. In single thin lenses, the curvature of the lens dictates the refraction angle that an incoming parallel light rays experience as it travels towards the focal point from its center to the edge of the lens, which is the effective focal length. In tunable lenses, the mechanical pressure builds up radially along the lens to change its shape and thereby alter the focal length of the lens [15]. When a droplet hangs from underneath a flat surface, it will experience two competing forces that act in opposing directions: the pulling force (gravity) acting to pull it down and the cohesive forces (surface tension) trying to hold the droplet up against the flat surface. The competing forces vary across the droplet where the liquid closest to the surface will remain almost stationary and the liquid molecules furthest away from the surface will be pulled downwards. This action is repeated across the transverse plane where the droplet is stretched almost into a parabola. As the result, for a transparent droplet, this difference in tensions across the lateral dimension forms a simple curved lens. On the other hand, a droplet placed on top of a flat surface will not experience such competing forces and produce a less curved lens.

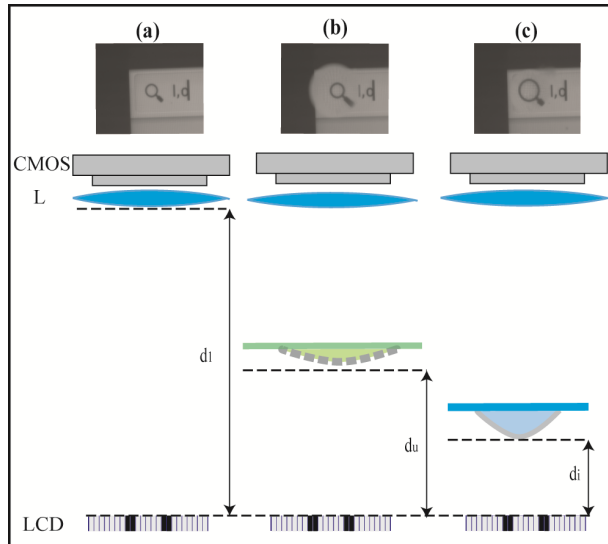


Fig. 1. Comparison of the magnification achieved without (a) and with a PDMS lens cured in an upright (b), and inverted (hanging droplet) position (c). The imaging lens (L) is maintained at a distance  $d_i$  away from the LCD screen (LCD) and a fixed distance from CMOS camera (CMOS) and the PDMS lenses positioned at imaging distance of  $d_u$  for the upright and  $d_i$  for the inverted hanging droplet lens. (a) shows the image of a magnifying glass displayed with just the imaging lenses L,  $d_{\text{lens}}$ . (b) and (c) shows the magnified image of a magnifying glass with horizontally and hanging droplet respectively. The hanging droplet (c) shows an image with approximately twice the magnification of the horizontal droplet (b).

We experimentally verified the effect of curvature on focal length and magnification by curing the same volume of PDMS droplet ( $\sim 100 \mu\text{l}$ ) in two different positions (inverted and upright). In Fig. 1(a), we show the imaging setup where a LCD screen is placed at a fixed distance,  $d_{\text{lens1}}$  from a CMOS camera. The LCD displays an intensity pattern that is imaged onto the camera with L1,  $f = 75 \text{ mm}$ . Figure 1(b) shows the LCD intensity pattern imaged using L1. Next, we placed the two PDMS lenses, labelled as shown in Fig. 1(b) and Fig. 1(c), between the LCD screen and camera. Since the two PDMS lenses have a shorter focal length (upright (b) = 40 mm and inverted (c) = 10 mm) than the imaging lens, the image will be magnified as a result as shown in Eq. (1).

$$M = -\frac{d_1}{d_{u,i}}, \quad (1)$$

Figure 1(b) and 1(c) corresponds to the images captured with PDMS lenses fabricated with in the upright and inverted geometry. By comparing the two images, it is evident that the hanging droplet produces a lens with shorter focal length and higher magnification. This means that the shape of the droplet is preserved during curing. Next we explain how this hanging method is further exploited to adjust the lens curvature during fabrication.

### 2.1. Adding more hanging droplets

Additive manufacturing is the sequential layering of materials to create complex three dimensional structures over time. The process is best exemplified by 3D printing technology. We have devised a similar but yet distinct variant of this approach by successively depositing, inverting and curing smaller volume droplets onto already cured PDMS droplets. In this manner, each subsequent droplet is bound to a curved PDMS surface by surface tension which decreases as each layer is added. Thus, the curvature of the final cured PDMS surface inevitably increases to produce lenses with shorter focal lengths. Through our experiments, we empirically found a direct dependence between that the change in the focal length of the lens and the amount (volume) of deposited droplet. A larger droplet will result in a bigger

step change of the focal length, whereas a smaller amount of droplet achieves a finer step change in the focal length of the lens. With our droplet dipping method, we were able to control the change in the focal length at a maximum of 15 mm and the minimum of 1 mm with a variation of 0.5 mm. In our experiments, we fixed the droplet volume to around 100  $\mu\text{l}$ . One key advantage of this technique is that no mold is used and the droplet is subjected to almost uniform tension forces as it cures. Hence, it eliminates the mechanical defects that can occur from mold injection and stamping processes.

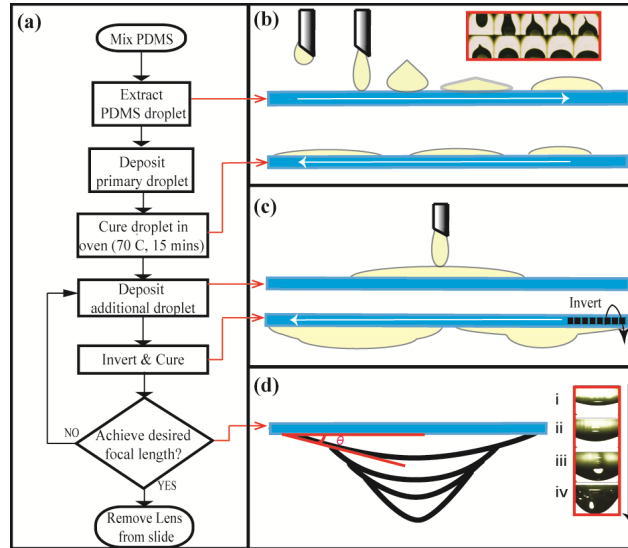


Fig. 2. Inverted additive fabrication from the primary droplet to the additional droplets. (a) Flow chart of the fabrication process. (b) Sequence of steps from the extraction to deposition (inset experimental image) of the PDMS droplet and to the subsequent spread on the surface to form the initial base (white arrow indicate direction of steps). (c) Additional droplet added to the PDMS base and direct inversion of the slide. (d) Sequential deposition of additional inverted droplets increases the curvature of the PDMS layer and increases the apex angle ( $\theta$ ) as shown in the inset images (i) to (iv).

In Fig. 2(a), the flow chart lists each fabrication step. The individual fabrication processes are categorized into four actions: extract, deposit, invert and cure. The initial mixing process follows the typical soft lithography PDMS recipe (2 part - Sylgar 184, Corning), which is to mix the PDMS base with the curing agent by weight at a ratio of 10:1. After mixing and resting the PDMS to remove residue bubbles, an 18–21 gauge hypodermic needle (Terumo) is dipped vertically into the mixture to extract a small drop ( $\sim 100 \mu\text{l}$ ). The extracted high viscosity PDMS droplet is allowed to slide slowly onto a microscope glass slide. The first deposited drop is left on top of the microscope glass slide in an oven at  $70^\circ\text{C}$  for 15 minutes, Fig. 2(b). This initial deposit serves as a support base for the second layer. The second droplet is layered onto the support layer and immediately inverted in Fig. 2(c). Without any external lateral force, the rate of fluid flow on a smooth surface is dependent on the viscosity of the solution. Since the pre-cured PDMS is highly viscous ( $\sim 3500$  centipoise) and the surface of the microscope slide is relatively smooth, the shape of the PDMS droplet is maintained throughout the duration of inversion. We empirically found that this approximates to 2 seconds between deposition and inversion through a sessile drop experiment (Fig. 2(b) inset). The inverted droplet is then placed in an oven for up to 15 minutes at  $70^\circ\text{C}$ . To shorten the focal length, we removed the sample from the oven and deposited a third layer of the same drop volume onto the previously cured PDMS lenses. The eventual droplet shape at the apex will resemble that of a parabola. This is due to the maximum surface tension that the droplet can hold before breaking up. In Fig. 2(d), we layered around four  $100 \mu\text{l}$  droplet, (i) to (iv), onto the initial supporting layer. At the layering of each droplet, the contact angle measured at

the apex of the lens monotonically increases: (i)  $14.5^\circ$ , (ii)  $19^\circ$ , (iii)  $25^\circ$  and (iv)  $37^\circ$ . Our qualitative assessment of the fabrication showed when more than two droplets are deposited, the repeatability of the fabrication reduced by 60% due to error in manual centering and inversion of the droplet.

### 3. Imaging

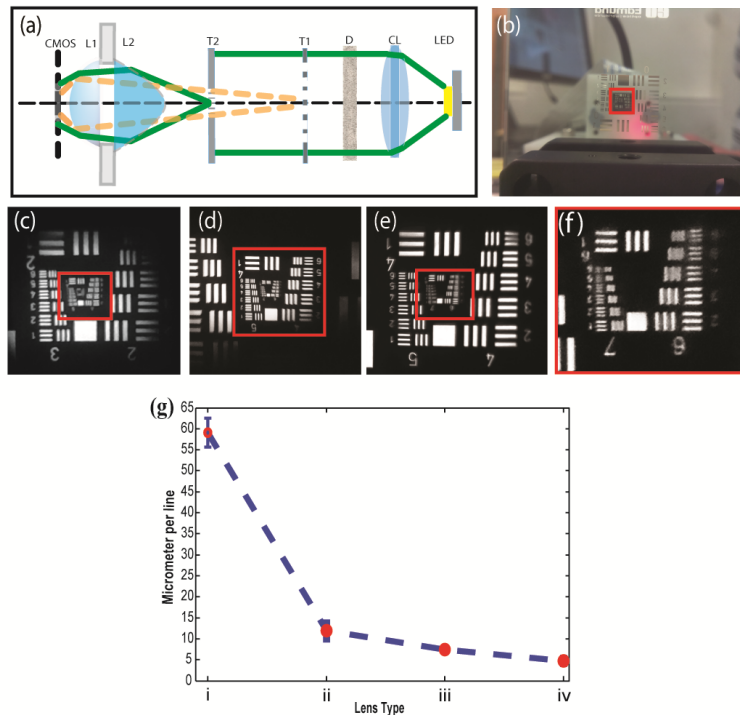


Fig. 3. Quantification of the imaging resolution of the PDMS lens. (a) shows the transmission light imaging where light emitted from the LED (green rays) is collimated and diffuses before undergoing diffraction (green solid line and orange dotted line) through the 1951 USAF resolution card (T1 and T2). L1 and L2 indicate the position of the camera imaging lens and PDMS lens respectively. CMOS is the imaging sensor used to capture the diffraction pattern. (b) shows the image taken with just L1. (c) to (f) show the image of the 1951 USAF resolution card taken for PDMS lenses (i) to (iv) shown in Fig. 2(d). The minimal resolvable lines on a USAF 1951 imaged by the PDMS lenses were plotted in (g). (c)–(f) have digital zoom  $\sim 4\times$ .

The optical resolution of an imaging system is typically defined by smallest resolvable structure. In Fig. 3, light emitted by an LED is collimated by a collector lens ( $f = 50$  mm) that is diffused to provide an even illumination over the 1951 USAF resolution card. The resolution card consists of binary transmission gratings with width from sizes  $2000\ \mu\text{m}$  to  $2.19\ \mu\text{m}$ . The diffracted light from the gratings are collected by the PDMS lens (L2) and then relayed onto the CMOS sensor by the camera lens (L1). The larger gratings (T1) will diffract light at a smaller angle than smaller grating (T2). In our experiment, we attached our lens directly onto a 5 megapixel CMOS imaging sensor (OmniVision, OV5647 from Raspberry Pi) with its in-built imaging lens. In Fig. 3(c) to 3(f), we show images captured with four PDMS lenses corresponding to Fig. 2(d) (i) to (iv). The smallest resolvable gratings substantially reduced from 55.68 micrometers in (i) to 3.91 micrometers (iv). This corresponds to the maximum magnification of 160  $\times$ . Interestingly, from Fig. 3(g), we observed the imaging resolution is increased by almost an order of magnitude in imaging resolution with just the second layered PDMS droplet. The diameter of the entrance pupil of lenses (i) to (iv) measured using a ruled graticule and CCD camera were 8.5 mm, 5.8 mm, 2.5 mm and 1.4 mm respectively. The focal length of each lens measured using a collimating

light source was found to be approximately 35 mm, 10 mm, 3.5 mm and 2 mm which results in an estimated numerical aperture (NA) of 0.12, 0.29, 0.31 and 0.35 for lenses (i) to (iv) respectively. Since the volume of droplet in our experiment is fixed at 100  $\mu\text{l}$ , we hypothesize that the second droplet was sufficient to reach a curvature close to its optimal, as attained in lens (iv).

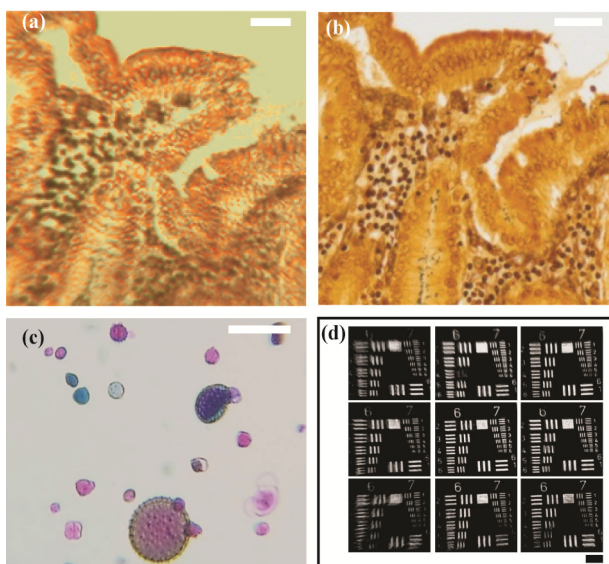


Fig. 4. Brightfield imaging with PDMS lens on an upright Olympus BX 51 microscope. (a) shows the image of a slice of human colon from a fixed pathology slide taken with the PDMS lens. (b) shows the image of the same sample taken with a  $10\times 0.25$  NA microscope objective. (c) shows image of pollen grains on a fixed slide (Carolina Biological Supply). (d) shows grating elements on a USAF 1951 target card group (6, 7) taken at different transfer position that are spaced  $200\ \mu\text{m}$  apart of each other. Scale Bar (a), (b), (c), (d)  $50\ \mu\text{m}$ .

In addition to the resolution measurement, we qualitatively compared the performance of the PDMS imaging lens (iv) with a conventional microscope. We used fixed tissue and pollen grain samples for quantitative comparison. For convenience, we chose the highest power PDMS lens (shortest focal length). In order to objectively match the imaging requirements, we performed imaging on a commercial microscope system (Olympus BX51). The PDMS lens is placed between the sample and a  $4\times$  microscope objective. The  $4\times$  objective lens together with the tube lens relays the image onto the 5 megapixel digital camera. For comparison, we took an image of the same sample with a  $10\times$  microscope objective. The image of the pathology slide taken with the PDMS lens and  $10\times$  ( $0.25$  NA) microscope objective lens are shown in Fig. 4(a) and 4(b) respectively. In Fig. 4(c), we also show the ability of the PDMS lens to image single pollen grains. The images taken by the PDMS lens here are shown to be almost comparable in quality to existing commercial microscopes. From Fig. 4 (a), 4(c), there are noticeable distortions at the periphery of the lens. This is likely due to the non-aspherical shape of our lens with additional more droplets deposition. We qualitatively verify the distortion of the lens by place the USAF 1951 target (group 6, 7) in 9 positions, each  $200\ \mu\text{m}$  apart. The visibility of the grating element (7, 3) is 65% at the highest in the center of the lens and degrades down to 21% at  $200\ \mu\text{m}$  off center. We have also quantified the point spread function (PSF) of the lens using  $1\ \mu\text{m}$  diameter fluorescence microspheres. From the cross-section of the intensity distribution (not shown) is measured to have a PSF (full width half-maximum) of approximately  $2.4\ \mu\text{m}$ .

#### 4. Light collimation

Next, we quantify the emitted light from the LED with and without the PDMS lens. To perform a local measurement of the intensity, we constructed a confocal-light collection

system. In Fig. 5(a), a multimode optical fiber with a NA of 0.22 (Thorlabs AFS50 model) is positioned orthogonally to the LED. Light emitted from the LED enters the input aperture of the optical fiber and propagates through the fiber to the input of the spectrometer. The optical fiber here acts like a pinhole light collector. Due to the planar surface on one side of the lens, we can directly mount it to the LED. Since the output of the fiber is linked to a spectrometer (Thor Labs CCS175 model), we can measure the total power and wavelengths of light transmitted through the lens. The LED used was an Avago Technologies ASMT-UWB1-NX3A2 model that was powered by a 9V battery in series with a 270  $\Omega$  resistor for the LED.

This produced sufficient brightness such that the spectrometer could register light intensities from the multimode optical fiber. The optical fiber was then aligned with the sample platform such that the tip of the optical fiber was just in contact with the top of the LED. These steps were taken to ensure that light intensity measurements would not be affected by incorrect orientation of the apparatus. The origin line (blue line) was defined at the point of contact between the LED/or lenses and the optical fiber. The optical fiber could be incrementally moved around the two orthogonal directions (vertical and horizontal) above the LED so as to sample the local intensity values. Since we are collimating a broadly diverging beam directly at its output, it makes sense to use PDMS lens with the shortest focal length of  $\sim 1$  mm.

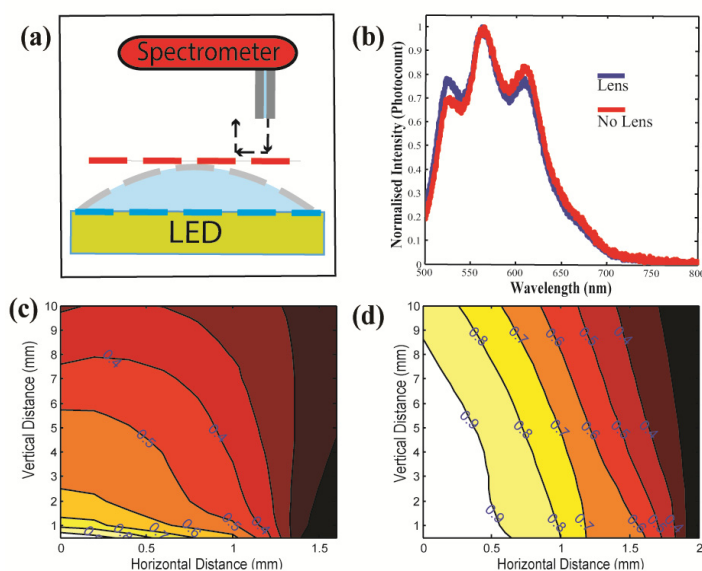


Fig. 5. Scheme for measurement of the lens for LED collimation with, and without an elastomeric lens. (a) shows the LED with PDMS lens and a fiber-coupled spectrometer setup. The origin point for the LED with and without PDMS lenses are indicated by dotted red and blue line, (b) shows the normalized spectrum of the emitted light output with (blue) and without (red) the PDMS lenses. (c) and (d) shows the cross-sectional contour plot of the total emitted light intensity (the sum of the intensity values obtained for each wavelength).

For measurement, the line of origin begins from the tip of the lens (red dotted line) for the case of collimation and the top of the LED surface (blue dotted line) for bare LEDs. The vertical axis was sampled in increments of 0.5 mm, whereas the horizontal axis was sampled in increments of 0.2mm. In both cases, the vertical sampling began at around 0.5 mm above the LED or lens. Figure 5(b) shows the transmitted wavelengths from the PDMS lens at the central axis indicating almost no chromatic aberration. The cross-section contour intensity plot in Fig. 5(c) and 5(d) showed that the PDMS lens substantially reduced the divergence of the emitted light. The intensity of the emitted light at 10 mm from the LED without the PDMS lens were shown to be reduced by approximately 40%, whereas with the PDMS lens,

there was only a reduction of 14%. Hence, this demonstrates that the PDMS lenses can be used to reduce the light diverging from the LED element.

## 5. Low cost dermascope

Clinical studies have shown that considerable risks (health and cost) associated with unnecessary biopsy and treatment interventions can be avoided using epiluminescence microscopy [2]. Commercial digital microscope costs around USD\$300-\$500 each. Their mobile counterpart costs well over ~USD \$100 and increases the footprint of smartphones substantially.

Here, we proposed that the addition of a single PDMS lens to a smartphone camera to transform it into a high performance mobile digital microscope platform. Typical dermascope operates as an epi-reflectance microscope which collects light that are reflected off the sample. With that in mind, we fabricated a simple microscope device using a 3D printer (ABS material, Up-Mini). The device includes a battery compartment, a lens window and two angled pedestals to hold the LEDs. The angled pedestals ensure that light from the two LEDs intersects at the imaging plane of the PDMS lens. In Fig. 6(a), we show the microscope device attached to a Nexus 4 smartphone that contains PDMS lens fabricated using the droplet technique described in Fig. 2(d) (ii). In Fig. 6(b), we carried out a comparison of the imaging performance on a 1951 USAF calibration card between a non-angled LED illumination (left) and an angled ( $20^\circ$ ) LED illumination (right) on the smartphone camera. A cross-section plot (not shown here) showed a 20% increase in contrast. Using the same imaging device, we imaged the skin of a human subject. Figure 6(c) shows the image of a fingertip taken without the microscope device and Fig. 6(d) showed the image of the fingertip magnified with the device. The highly undulating features such as fingerprint ridges and single sweat pores were clearly resolved using our microscope device. The combined cost and weight of the entire microscope device is only around US\$2 and weigh less than 0.5g.

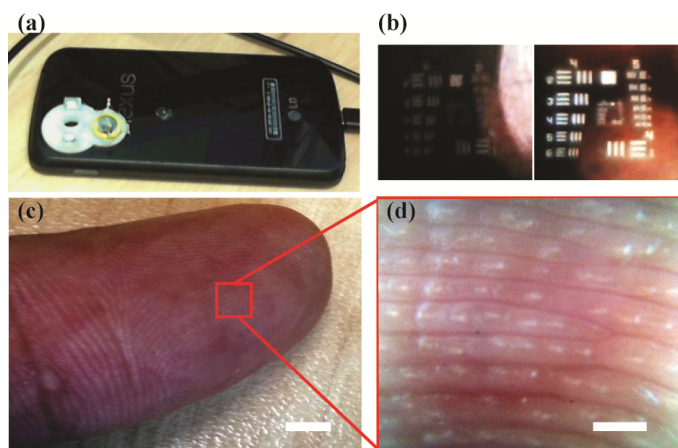


Fig. 6. Epi-reflectance imaging of stratum corneum layer of a human subject, with and without the PDMS 3D printed microscope device. (a) shows the microscope device attached to a Nexus 4 smartphone. (b) compares the imaging performance on a 1951 USAF resolution card between a non-angled LED illumination (left) and an angled ( $20^\circ$ ) LED illumination (right) on the smartphone camera resolving  $22\ \mu\text{m}$  line (Group 4,4). (c) shows the image of a fingertip taken without the microscope device and (d) showed the magnified image ( $\sim 60\times$ ) of the fingertip using the microscope attachment. Scale bar (c) 1 cm, (d)  $500\ \mu\text{m}$ .

## 6. Conclusion

In conclusion, we have systematically developed a novel lens fabrication method that achieves high performance lenses at almost zero cost. The hanging droplet technique only requires a flat surface (in this case a microscope slide) and a low temperature dry oven (up to  $200\ ^\circ\text{C}$ ). Our minimalistic approach means that the fabrication can be replicated in different

environments with low cost. Our current fabrication step is limited by the size of the dipping needle and the inversion process. In the next step, we envisioned that a finer process using simple fluidic control and exert a more precise control over the change in the focal length of the lens. This will increase the repeatability of the fabrication method for higher powered lens. Furthermore, there are noticeable aberrations along the periphery of the lens which is more apparent at higher magnification. While the use of field compensating optical elements could potentially reduce the distortion, we are considering to use computational optical algorithms [19] to overcome the aberrations. The fabricated PDMS lenses are shown to greatly increase both the imaging resolution of a miniature camera system (up to 160x magnification) and maintains a fairly constant LED illuminating field. Using a commercial 3D printer, we fabricated a complementary microscope attachment for the lenses with accompanying LED illuminators. The entire microscope with magnifying power of  $\sim 60\times$ , takes up a footprint approximately  $\sim 30 \times 15 \times 5$  mm, which is at nearly two times smaller than any current commercial mobile microscope system. The parts are disposable and cost around  $\sim$ US\$2. The simplicity of our technique could bring about a new generation of low-cost, high performance lenses for the masses. Currently, this technique is a passive fabrication process which can be slow. Hence, the next step will be to refine the steps to develop a more active, parallel processing technique that will lead to high production volumes in shorter time frames.

### **Acknowledgments**

We acknowledge the help from Miss. Sjoukje Schoustra, Miss. Ana Andres-Arroyo for acquisition of images and useful discussions with Dr. Gwen Allison, Mr. Neil Radford, and Mr. Christopher Pugmire at Innovation ANU. We also thank Dr. Andrew Parker, Department of Anatomical Pathology, St. Vincent's Hospital, Sydney. A patent covering the fabrication technology in section 2 has been filed, AUS PAT: 2014900293.